RAA 2021 Vol. **21** No. **4**, 83(10pp) doi: 10.1088/1674-4527/21/4/83

http://www.raa-journal.org *http://iopscience.iop.org/raa*

***R**esearch in*
***A**stronomy and*
***A**strophysics*

The Mg II absorption line systems in quasar spectra from the Large Sky Area Multi-Object Fiber Spectroscopic Telescope

Zhi-Fu Chen[1,2,3], Huan-Chang Qin[2], Yan-Chun Gao[1], Run-Jin Gui[1], Zhe-Geng Chen[1] and Ting-Ting Pang[1]

[1] College of Mathematics and Physics, Guangxi University for Nationalities, Nanning 530006, China; *zhichenfu@126.com*
[2] School of Information Engineering, Baise University, Baise 533000, China
[3] Key Laboratory for Ionospheric Observation and Simulation, Guangxi University for Nationalities, Nanning 530006, China

Received 2020 June 30; accepted 2020 September 27

Abstract Making use of quasar spectra from LAMOST, in the spectral data around the Mg II emission lines, research described in this paper has detected 217 Mg II narrow absorption lines (NALs) with $W_r^{\lambda 2796} \geq 3\sigma_w$ and $W_r^{\lambda 2803} \geq 2\sigma_w$ in a redshift range of $0.4554 \leq z_{\rm abs} \leq 2.1110$. For quasars observed by both LAMOST and SDSS, we find that 135 Mg II NALs were obviously observed in the LAMOST spectra, 347 Mg II NALs were were apparent in the SDSS spectra, and 132 Mg II NALs were clearly present in both the SDSS and LAMOST spectra. The missed Mg II NALs are likely ascribed to low signal-to-noise ratios of corresponding spectra. Among the Mg II NALs obviously observed in SDSS or LAMOST spectra, eight Mg II NALs were significantly changed with $|\Delta W_r^{\lambda 2796}| \geq 3\sigma_w$ in time intervals of $\Delta {\rm MJD}/(1+{\rm z_{em}}) = 359 - 2819$ d.

Key words: line: identification — quasars: absorption lines — quasars: general

1 INTRODUCTION

Shortly after the discovery of quasars (e.g., Bahcall & Salpeter 1965; Bahcall et al. 1966; Bahcall & Salpeter 1966), quasar absorption lines (QALs) were found in the ultraviolet (UV)-optical spectra of quasars. Nowadays, QALs are very common in quasar spectra, and have been widely used to investigate the physical conditions associated with quasar themselves or with the quasars' intervening galaxies (the foreground galaxies far from quasar systems). The strengths of the QALs are mainly determined by the column densities of the absorbing gas, therefore, the detections of QALs do not depend on quasar emissions. In theory, QALs would be imprinted in the spectra of quasars so long as continuum emissions from the central regions of quasars pass through foreground gas clouds with suitable column densities before they reach the observers. Therefore, QALs are an important probe for the universe, and represent a valuable tool to investigate the properties of quasars and galaxies.

Mg II$\lambda\lambda$2798,2803 resonance doublets are good tracers that reflect the properties of neutral gas and low ionization gas (e.g., Lanzetta & Bowen 1990; Hamann 1997; Rao & Turnshek 2000), since they have strong oscillator strengths. In addition, the long rest wavelengths of the Mg II absorption doublet allow ground-based telescopes to track them with $z < 0.2$. Therefore, Mg II QALs are commonly detected in UV-optical spectra of quasars. Mg II QALs have been found to be likely related to foreground galaxies (e.g., Bergeron 1986; Bergeron & Boissé 1991; Lundgren et al. 2009; Chen et al. 2010; Kacprzak et al. 2010; Farina et al. 2014), or to quasar systems themselves (e.g.; Vanden Berk et al. 2008; Shen & Ménard 2012; Chen et al. 2018a). The Mg II QALs formed within foreground galaxies are often called intervening QALs, which generally have absorption line redshifts much less than emission line redshifts ($z_{\rm abs} << z_{\rm em}$), and the ones formed within the quasar system themselves are often called associated QALs, which generally have $z_{\rm abs} \approx z_{\rm em}$. The associated Mg II QALs have the potential to reveal information on quasar's outflows/inflows, host galaxies, environments, circumgalactic medium and so on (e.g., Bowen et al. 2006; Shen & Ménard 2012; Farina et al. 2014; Chen 2017; Chen et al. 2018a). The intervening Mg II QALs have the potential to reveal information on galactic disks, outflows/inflows, dwarf galaxies (e.g., Le Brun et al. 1993;

Charlton & Churchill 1996; Mo & Miralda-Escude 1996; Tinker & Chen 2008; Nestor et al. 2011), etc.

In the last two decades, the number of quasar spectra has dramatically increased after the advance of large spectroscopic surveys including the Sloan Digital Sky Survey (SDSS, York et al. 2000). The SDSS project has gathered quasar spectra in the wavelength range of $\lambda \approx 3600$ — 10000 Å (Abazajian et al. 2009; Alam et al. 2015) at a resolution of $R \approx 2000$. Taking advantage of quasar spectra from the SDSS, many groups have compiled large samples of Mg II QALs (e.g., Nestor et al. 2005; Lundgren et al. 2009; Quider et al. 2011; Seyffert et al. 2013; Zhu & Ménard 2013; Chen et al. 2015b, 2018a). The Large Sky Area Multi-Object Fiber Spectroscopic Telescope (LAMOST) is located at Xinglong Observatory, in China, which is a reflecting Schmidt telescope with effective aperture of 4 m and equipped with 4000 fibers (e.g., Cui et al. 2012; Zhao et al. 2012). The LAMOST quasar survey was carried out as part of the LAMOST ExtraGAlactic Survey following the regular survey in September 2012 (LEGAS; Zhao et al. 2012), which gathered quasar spectra in wavelength range of $\lambda \approx 3800 \sim 9100$ Å at a resolution $R \approx 1800$. Both coverage wavelength and resolution of the LAMOST quasar spectra are similar to those of SDSS. SDSS quasar spectra have been widely exploited to search for Mg II QALs, however, no single dedicated survey of QALs has been carried out in the LAMOST quasar spectra up to now. In this paper, we utilize the LAMOST quasar spectra to systematically search for associated Mg II QALs.

The outline of this paper is as follows. Section 2 describes the quasar sample and spectral analysis, Section 3 is for the results and discussions, and Section 4 is a brief summary.

2 QUASAR SAMPLE AND SPECTRAL ANALYSIS

LAMOST carried out a pilot survey in October 2011, and began regular surveys from September 2012 until June 2017 (e.g., Wu et al. 2010a,b; Luo et al. 2012, 2015). Utilizing Data Releases 1 – 5 of quasar catalogs from LAMOST, Ai et al. (2016), Dong et al. (2018) and Yao et al. (2019) compiled 43 109 quasars through checking the LAMOST spectra. In this paper, we rely on the LAMOST spectra of these 43 109 quasars to search for Mg II QALs around Mg II emission lines.

This paper mainly aims to search for associated Mg II QALs with line width less than a few hundred $\mathrm{km\,s^{-1}}$ (NALs, narrow absorption lines) in the spectral data around Mg II emission lines. Therefore, combining the coverage wavelength of the LAMOST spectra, we first reduce the parent sample of the LAMOST quasars with $3600/2800 < (1 + z_{\rm em}) < 9300/2800$. In terms of the statistical results

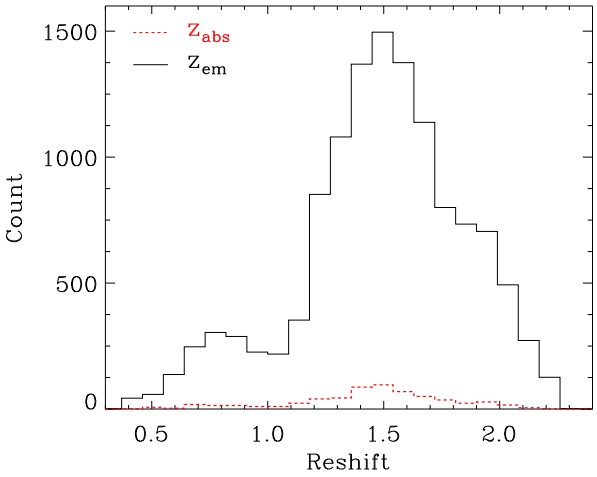

Fig. 1 The black solid line is for the redshifts of quasar systems ($z_{\rm em}$) used to search for Mg II NALs, and the red dashed line represents the redshifts of Mg II NALs ($z_{\rm abs}$).

of Chen & Pan (2017), most of the associated Mg II QALs are located within a velocity [1] range of $\upsilon_r < 2000\ \mathrm{km\,s^{-1}}$. Some outflow Mg II NALs might have been accelerated to high velocities by quasar radiations. We conservatively search for Mg II NALs in a wide velocity range, namely, from the blue wings $\upsilon_r = 10\,000\ \mathrm{km\,s^{-1}}$ until the red wings of Mg II emission lines (e.g., Chen et al. 2018a). This wide velocity range should contain the vast majority of outflow Mg II NALs with high velocity, although a few outflow Mg II NALs with $\upsilon_r > 10\,000\ \mathrm{km\,s^{-1}}$ will be outside our survey of QALs. In addition, we also constrain the quasars with median signal to noise ratio $(\mathrm{S/N}) > 3\ \mathrm{pixel^{-1}}$ in the surveyed spectral region (e.g., Chen et al. 2018a). Based on these two limits, the parent sample of the LAMOST quasars is reduced from 43 109 quasars to 12 317 quasars. Figure 1 displays the emission line redshifts of the 12 317 quasars with a black solid line.

We adopt the methods utilized by Chen et al. (2015b) and Chen et al. (2018a) to search for Mg II NALs. The main processes are described as follows.

1. The pseudo-continuum fits. We invoke a cubic spline plus multi-Gaussian functions to fit the underlying continuum and emission lines of quasar spectra, where the multi-Gaussian functions mainly account for the broad absorption features and/or the emission lines. The fitting results are often called pseudo-continuum. In our experience, a narrow Mg II emission line is difficult to distinguish from a broad one for most of the quasar spectra (e.g. Chen et al. 2019a), except for some quasars hosting strong narrow Mg II emission components. During the process of fitting the pseudo-continuum and the Mg II NAL surveys (next step), we visually inspect the fitting results one by one. For the

[1] $\beta \equiv \frac{\upsilon_r}{c} = \frac{(1+z_{\rm em})^2-(1+z_{\rm abs})^2}{(1+z_{\rm em})^2+(1+z_{\rm abs})^2}$, where the c is the speed of light.

bad fits, we will fit these spectra again by adjusting the original parameters of the Gaussian functions used to describe the emission/absorption lines.

The spectra are normalized by the pseudo-continuum fits, including the flux and flux uncertainties. The Mg II NALs are searched in the normalized spectra. This paper mainly focuses on the narrow absorption lines, which usually have line widths less than a few hundred $\mathrm{km\,s^{-1}}$. Therefore, we disregard the broad absorption lines (BALs), which often exhibit continual absorption features with widths $> 2000\ \mathrm{km\,s^{-1}}$ at depths <10% under the pseudo-continuum fit (e.g., Weymann et al. 1979). As two examples, Figure 2 displays the spectra of quasars J125058.11+570921.7 and J112654.96+163136.3, which are overplotted with the pseudo-continuum fits.

2. The Mg II NAL surveys. Absorption lines are surveyed in normalized spectra. The surveys are controlled by the separations of Mg II doublets, which are varied with redshifts. Each Mg II doublet candidate is fitted with two Gaussian functions. The fitting results are visually inspected. As examples, Figure 2 also displays the fitting results of three Mg II NALs with $z_{\rm abs} = 0.9188$, 1.4187 and 1.4729.
3. Absorption line redshifts and equivalent widths. We estimate the redshifts of Mg II NALs with the Gaussian function fitting center of Mg IIλ2796. The equivalent widths (W) of absorption lines are determined by the integrations of Gaussian function fitting profiles. The errors of equivalent widths (σ_w) are contributed from uncertainties in the spectral flux ($\sigma_{\rm flux}$) and the placements of pseudo-continuum fits ($\sigma_{\rm cont}$), namely, $\sigma_{\rm w}^2 = \sigma_{\rm flux}^2 + \sigma_{\rm cont}^2$. The $\sigma_{\rm flux}$ is estimated via

$$(1+z_{\rm abs})\sigma_{\rm flux} = \frac{\sqrt{\sum_{i=1}^{N} P^2(\lambda_i-\lambda_0)\frac{\sigma_{{\rm flux},i}^2}{f_{{\rm flux},i}^2}}}{\sum_{i=1}^{N} P^2(\lambda_i-\lambda_0)}\Delta\lambda, \quad (1)$$

where $P(\lambda_i - \lambda_0)$ is the line profile centered at λ_0, $f_{{\rm flux},i}$ is spectral flux, $\sigma_{{\rm flux},i}$ is spectral flux uncertainty and the summation is over 3σ line widths. The $\sigma_{\rm cont}$ is related to placement of the pseudo-continuum fit and the line width of absorption line near the pseudo-continuum fit ($\lambda_{\rm max} - \lambda_{\rm min}$), namely, $\sigma_{\rm cont} \propto (\lambda_{\rm max} - \lambda_{\rm min})\sigma_{\rm pf}$ (e.g.; Misawa et al. 2014; Chen et al. 2015a). Accounting for S/N of the absorption line, we estimate the $\sigma_{\rm cont}$ by

$$\sigma_{\rm cont} = \frac{A(\lambda_{\rm max} - \lambda_{\rm min})}{\rm S/N}, \quad (2)$$

where the calibration parameter A is estimated by fitting the pseudo-continuum multiple times around the absorption line, and the S/N is estimated with the methods applied by Qin et al. (2013). See Qin et al. (2013) for the detailed calculation of S/N of the absorption line.

In the LAMOST spectra of 12 317 quasars used to search for Mg II NALs, we detect 217 Mg II NALs with $W_r^{\lambda2796} \geq 3\sigma_w$ and $W_r^{\lambda2803} \geq 2\sigma_w$, whose parameters are listed in Table 1. Among these 12 317 quasars, 6427 quasars have been spectroscopically observed by SDSS. In the same surveyed spectral regions, for the 6427 quasars observed by both LAMOST and SDSS, Chen et al. (2015b) detected 347 Mg II NALs with $W_r^{\lambda2796} \geq 3\sigma_w$ and $W_r^{\lambda2803} \geq 2\sigma_w$ from the SDSS spectra, but this paper only detects 135 Mg II NALs with $W_r^{\lambda2796} \geq 3\sigma_w$ and $W_r^{\lambda2803} \geq 2\sigma_w$ from the LAMOST data. Among the 135 Mg II NALs imprinted in the LAMOST spectra and with $W_r^{\lambda2796} \geq 3\sigma_w$ and $W_r^{\lambda2803} \geq 2\sigma_w$, 132 Mg II NALs were visible in the SDSS spectra (Chen et al. 2015b) as well, but the other three Mg II NALs were missed by Chen et al. (2015b). Among the 347 Mg II NALs present in the SDSS spectra and with $W_r^{\lambda2796} \geq 3\sigma_w$ and $W_r^{\lambda2803} \geq 2\sigma_w$, $347 - 132 = 215$ Mg II NALs were missed by this paper. For the 215 (or 3) Mg II NALs identified in the SDSS (or LAMOST) spectra and with $W_r^{\lambda2796} \geq 3\sigma_w$ and $W_r^{\lambda2803} \geq 2\sigma_w$, which were missed by this paper (or by Chen et al. 2015b), we also estimate their equivalent widths or the upper limits of equivalent widths from the LAMOST (or SDSS) spectra. The results of the 215 Mg II NALs missed by this paper are also provided in Table 1. The redshifts of the 135 Mg II NALs detected by this paper and the 215 Mg II NALs missed by this paper are depicted in Figure 1 with a red dashed line, which are in the range $0.4554 \leq z_{\rm abs} \leq 2.1110$.

3 RESULTS AND DISCUSSIONS

Section 2 has affirmed that the detection rate [2] of Mg II NALs is obviously lower in the LAMOST spectra than that in the SDSS spectra. This would be mainly ascribed to the lower S/N of the LAMOST spectra relative to the SDSS spectra. Of course, the evolution of Mg II NALs might also play a role in the low detection rate of Mg II NALs in the LAMOST spectra. Figure 3 features the detection rates of Mg II NALs as a function of S/N for the LAMOST spectra, which clearly implies that the detection rate of weak Mg II NALs is obviously dependent on the S/N of spectra. For example, detection rates of Mg II NALs with $W_r^{\lambda2796} > 0.2$ Å (or $W_r^{\lambda2796} > 0.5$ Å) increase rapidly with S/N when $\rm S/N < 12$.

[2] The ratio between the quasar numbers detected with at least one Mg II NAL and used to search for Mg II NALs.

Table 1 Catalog of Mg II Absorption Line Systems

OBSID	LAMOST name	Spectra name	z_{em}	z_{abs}	$W_r^{\lambda2796}$ Å	$W_r^{\lambda2803}$ Å	v_r km s^{-1}
18809175	081001.59+203112.8	spec-55916-F5591604_sp09-175.fits.gz	1.8350	1.8187	1.72±1.04	0.77±1.03	1846
20203110	105817.30+503819.9	spec-55919-F5591906_sp03-110.fits.gz	1.5587	1.5573	0.61±0.45	0.56±0.27	11
20203110	105817.30+503819.9	spec-55919-F5591906_sp03-110.fits.gz	1.5587	1.5571	0.58±0.30	0.46±0.28	35
20702092	092746.51+105659.5	spec-55920-F5592004_sp02-092.fits.gz	1.5681	1.5122	0.90±0.90	0.59±0.39	6168
20711143	093421.29+150813.3	spec-55920-F5592004_sp11-143.fits.gz	1.9480	1.8988	2.34±2.34	0.25±6.51	5068
26204165	114856.81+573820.4	spec-55931-F5593101_sp04-165.fits.gz	1.5660	1.5692	0.66±0.70	0.42±0.29	-1439
32615099	125058.11+570921.7	spec-55951-F5595106_sp15-099.fits.gz	0.9080	0.9118	1.25±0.53	0.99±0.63	-1037
42406249	145147.40-012735.2	spec-55976-F5597606_sp06-249.fits.gz	1.3270	1.3272	0.54±0.54	0.24±1.18	-839
42504022	112733.45+543607.9	spec-55976-F5597612_sp04-022.fits.gz	1.6304	1.6360	1.05±0.57	0.81±1.39	-1288
77204198	010135.45+071021.1	spec-56240-EG010249N073002F_sp04-198.fits.gz	1.3529	1.3243	0.57±0.10	0.31±0.17	3668
103205116	093442.26+224439.5	spec-56299-HD093359N232714F01_sp05-116.fits.gz	1.7476	1.6787	1.84±0.42	1.65±0.35	6950
105903028	082547.84+393638.7	spec-56304-HD083110N401329F01_sp03-028.fits.gz	1.4756	1.4376	0.35±0.34	0.40±3.71	4809

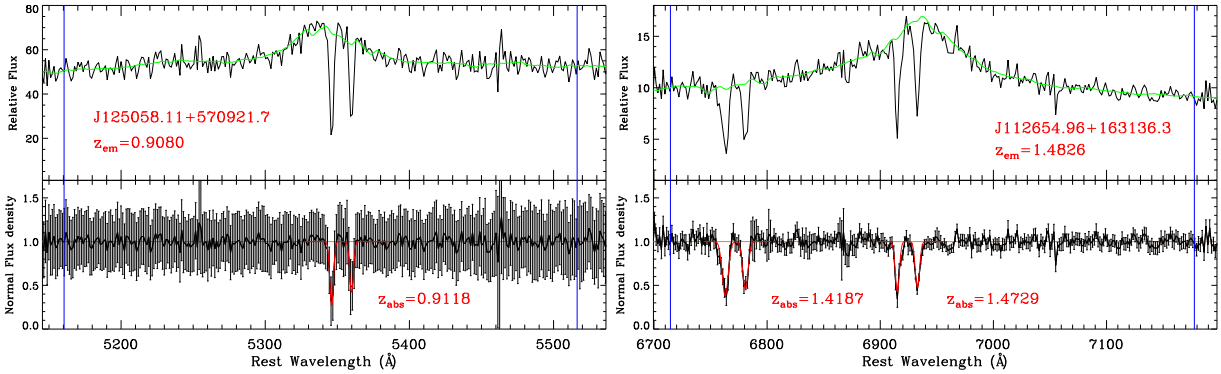

Fig. 2 The spectra of quasars J125058.11+570921.7 and J112654.96+163136.3 with redshifts $z_{\rm em} = 0.9080$ and 1.4785, respectively. The blue vertical lines are the boundaries of surveyed spectral regions of Mg II NALs. The green lines are the pseudo-continuum fits. The red lines are the Gaussian function fits of the Mg II NALs.

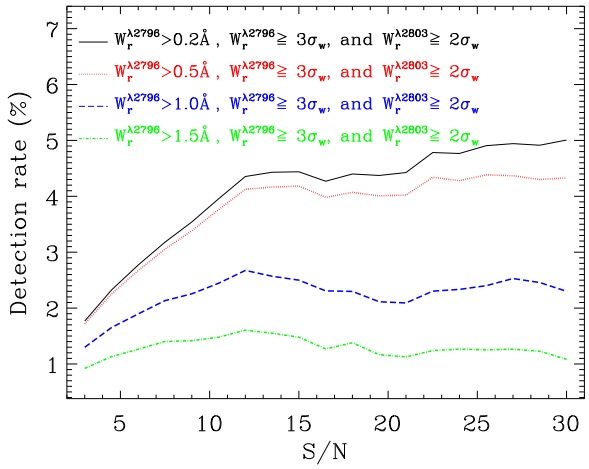

Fig. 3 Ratios between the number of quasars detected with at least one Mg II NAL and those used to search for Mg II NALs. Colored lines represent the Mg II NALs with different equivalent widths.

Section 2 has shown that there are 132 Mg II NALs with $W_r^{\lambda2796} \geq 3\sigma_w$ and $W_r^{\lambda2803} \geq 2\sigma_w$, which were detected from both the SDSS and LAMOST spectra. For these 132 Mg II NALs, Figure 4 compares the distributions of the S/N of quasar spectra and the equivalent widths of Mg II NALs. It is clearly seen that S/N values of the LAMOST spectra (median $\rm S/N = 14.3$) are slightly smaller than those of the SDSS spectra (median $\rm S/N = 16.7$). The Kolmogorov-Smirnov (KS) tests suggest that S/N values of the SDSS spectra are obviously different from those of the LAMOST spectra, but the equivalent widths of Mg II NALs measured from the SDSS spectra are similar to those measured from the LAMOST spectra. In addition, the right panel of Figure 4 clearly indicates that the weak Mg II NALs are difficult to detect in spectra with low S/N. For example, no Mg II NALs with $W_r^{\lambda2796} < 0.7$ Å were detected in spectra with $\rm S/N < 7$.

Figure 5 also compares the distributions of S/N of quasar spectra and the equivalent widths of Mg II NALs, where Mg II NALs are only detected in the SDSS spectra. It is clearly seen that the S/N values of the LAMOST spectra (median $\rm S/N = 6.4$) are much smaller than those of the SDSS spectra (median $\rm S/N = 18.9$). Although the KS-test suggests that the distribution of equivalent widths measured from the SDSS spectra is different from that measured from the LAMOST spectra, the median $W_r^{\lambda2796}$ measured from the LAMOST spectra (0.92 Å) is consistent with that measured from the SDSS spectra (0.93 Å). In addition, in terms of the equivalent widths measured

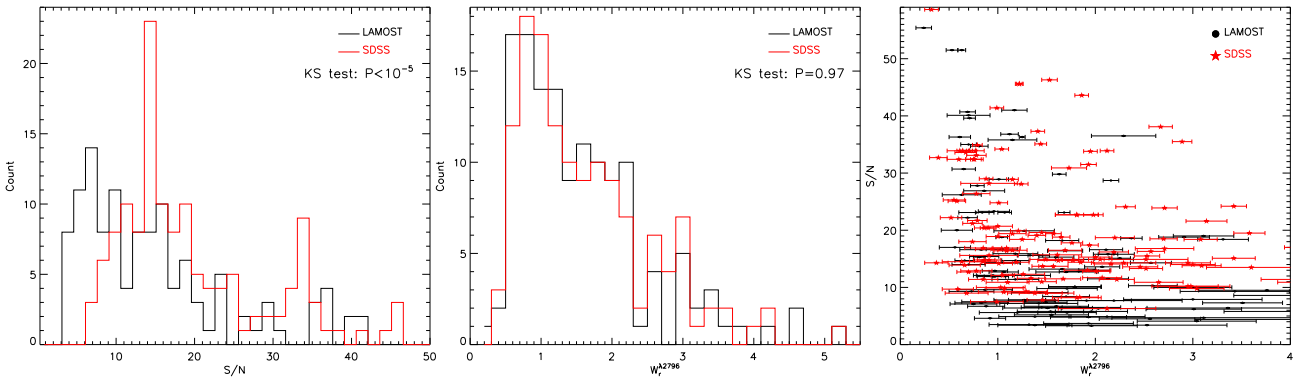

Fig. 4 Comparisons of the S/N of quasar spectra and equivalent widths of Mg II NALs, where the Mg II NALs were detected from both the LAMOST and SDSS spectra. The *right panel* clearly shows that the weak Mg II NALs are mainly detected in spectra with high S/N.

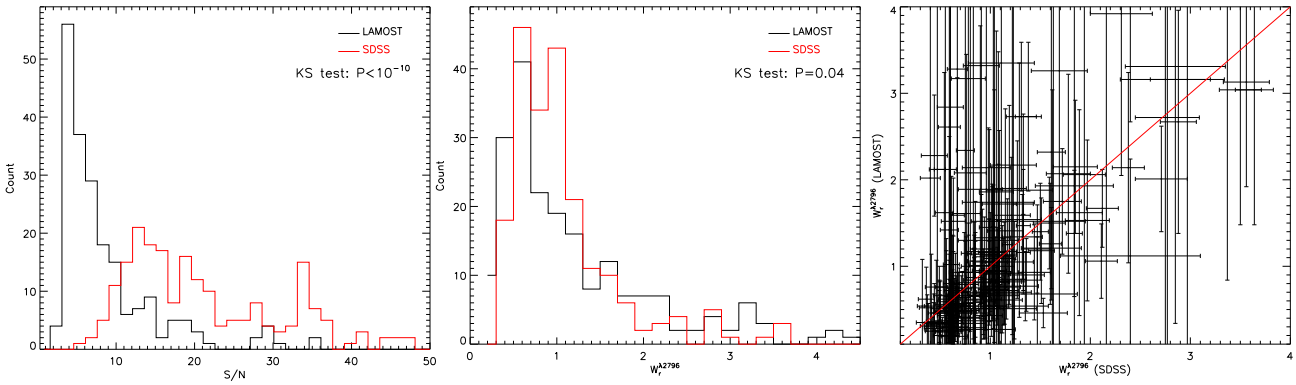

Fig. 5 Comparisons of the S/N of quasar spectra and equivalent widths of Mg II NALs, where the Mg II NALs were only detected from the SDSS spectra. $W_r^{\lambda2796}$(LAMOST) values are the equivalent widths directly measured from the LAMOST spectra or the $1\sigma_w$ upper limits of equivalent widths. The large σ_w measured from the LAMOST spectra are mainly ascribed to the low S/N of the LAMOST spectra (the black symbols in the right panel).

separately from the LAMOST and SDSS spectra, 83.7% of the Mg II NALs are consistent within 1σ error, and 97.6% of the Mg II NALs are consistent within 2σ error. Therefore, the low S/N of the LAMOST spectra would be the main reason why some Mg II NALs detected in the SDSS spectra were missed from the LAMOST spectra (see also Fig. 3).

3.1 Velocities and Equivalent Widths of Mg II NALs

Velocity offsets of absorbers are a convenient tool to distinguish the associated absorbers from the intervening ones. The Mg II NALs with $v_r < 2000$ km s^{-1} are often considered as associated absorption systems, while the Mg II NALs with $v_r > 2000$ km s^{-1} would be mainly dominated by the intervening absorption systems (e.g., Chen & Pan 2017). We search for Mg II NALs in the LAMOST spectral data with $v_r \leq 10\,000$ km s^{-1}. This wide surveyed region results in the sample of Mg II NALs detected from the LAMOST spectra, which contains not only associated Mg II NALs but also a significant number of intervening Mg II NALs. The black line in Figure 6 displays the velocities of the 217 Mg II NALs detected from the LAMOST spectra and with $W_r^{\lambda2796} \geq 3\sigma_w$ and $W_r^{\lambda2803} \geq 2\sigma_w$, which is similar to the results discovered

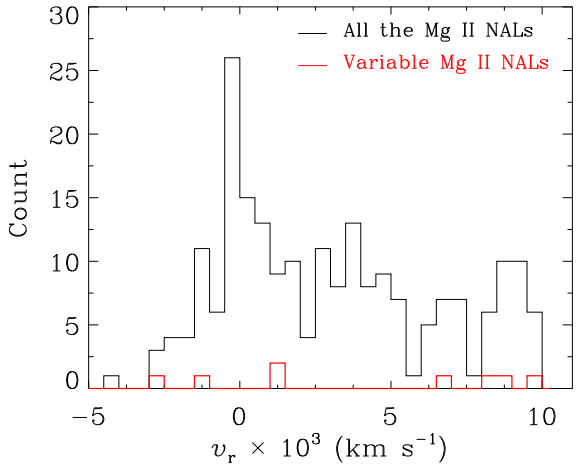

Fig. 6 Velocity offsets of Mg II absorption line systems. The black line is for all the 217 Mg II NALs detected by this paper, which clearly features a significant peak at $v_r \approx 0$. The red line is for the variable Mg II NALs.

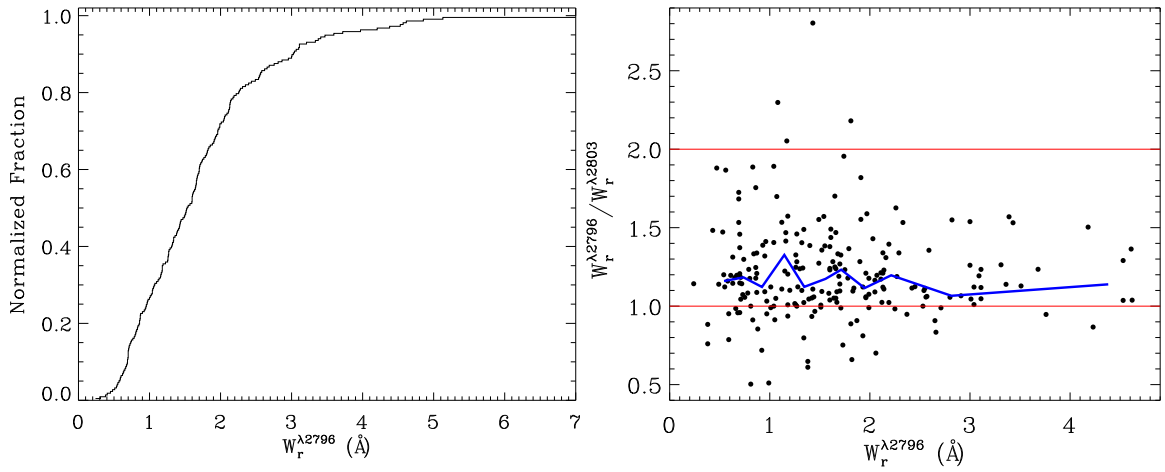

Fig. 7 Distributions of absorption strengths for the 216 Mg II NALs detected by this paper. *Left panel*: the y-axis has been normalized by the total number of Mg II NALs. *Right panel*: the red lines are for the theoretical limits of completely saturated (DR= $W_{\rm r}^{\lambda2796}/W_{\rm r}^{\lambda2803}=1$) and unsaturated (DR= $W_{\rm r}^{\lambda2796}/W_{\rm r}^{\lambda2803}=2$) absorption, respectively. The blue line is for the median values of DR as a function of $W_{\rm r}^{\lambda2796}$.

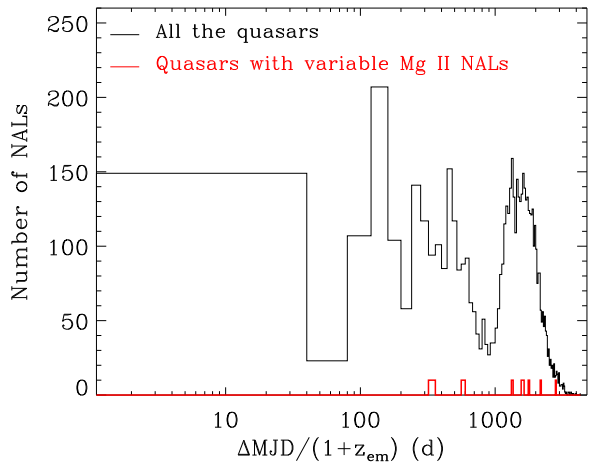

Fig. 8 Time intervals of the quasars between the LAMOST and SDSS observations. The black line is for all the quasars detected by both LAMOST and SDSS, and the red line is for the quasars having Mg II NALs with $|\Delta W_r^{\lambda2796}| \geq 3\sigma_w$, where y-axis values (the red line) have been multiplied by 10 for a convenient inspection.

from the much larger samples of Mg II NALs (e.g., Nestor et al. 2008; Wild et al. 2008; Chen et al. 2015b, 2018a). The significant excess around $v \approx 0$ would be mainly contributed from absorptions formed within the media surrounding quasars, such as quasar's host galaxies, clusters, outflows with low velocities and so on.

Figure 7 plots the absorption strengths of the 217 Mg II NALs detected by this paper. Both the distributions of the absorption strength (the left panel of Fig. 7) and the absorption strength ratios $DR = W_r^{\lambda2796}/W_r^{\lambda2803}$ (the right panel of Fig. 7) are similar to previous results (e.g., Quider et al. 2011; Chen et al. 2015b, 2018a). There are $\sim$ 97% of Mg II NALs with $W_r^{\lambda2796} \geq 0.5$ Å and $\sim$ 74% of Mg II NALs with $W_r^{\lambda2796} \geq 1$ Å. There are about 97% of the Mg II NALs whose absorption strength ratios are in a range of $1-\sigma_{\rm DR} \leq DR \leq 2+\sigma_{\rm DR}$, where 1 and 2 are the completely saturated and unsaturated absorption (Strömgren 1948), respectively.

3.2 The Mg II NALs with Multi-epoch Observations

Among the 12 317 quasars used to search for Mg II NALs in this paper, 6427 quasars were previously observed by SDSS. Figure 8 depicts the time intervals of the quasars between the LAMOST and SDSS observations. There are 5049 quasars that were repeatedly observed by LAMOST within a time interval $\Delta{\rm MJD}/(1+{\rm z_{em}}) > 1$ yr. Some Mg II NALs likely changed during this large time interval. For the 6427 quasars observed by both LAMOST and SDSS, we find that there are 347 Mg II NALs imprinted in the SDSS spectra, among which 132 Mg II NALs were also obviously observed in the LAMOST spectra ($W_r^{\lambda2796} \geq$

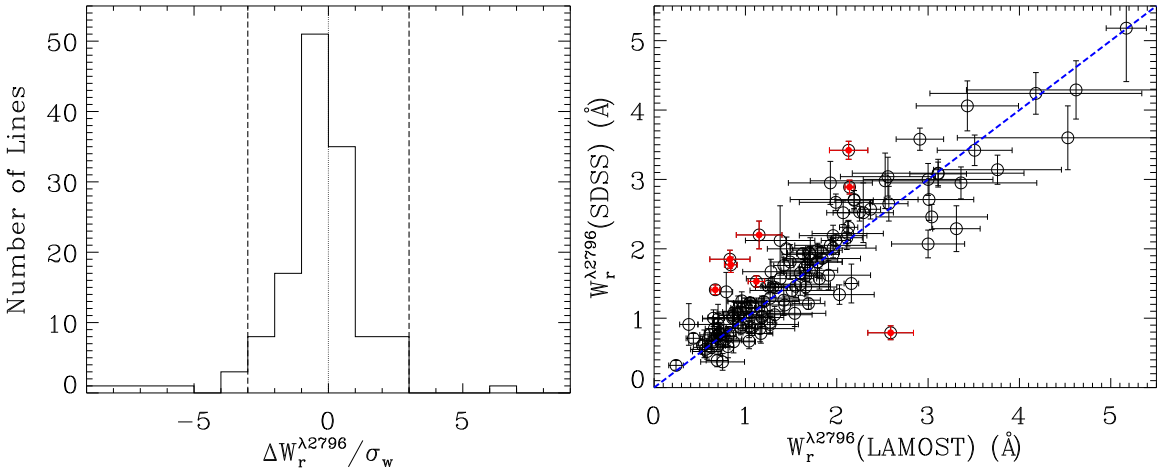

Fig. 9 Distribution of variations of absorption strengths between two-epoch observations. *Left panel*: Different absorption strengths that have been normalized by uncertainties. Vertical dotted and dashed lines represent $\Delta W_r/\sigma_w = 0$ and ± 3, respectively. *Right panel*: Red filled circles represent the variable Mg II NALs with $|\Delta W_r^{\lambda 2796}| \geq 3\sigma_w$, and the blue dashed line is the identity line.

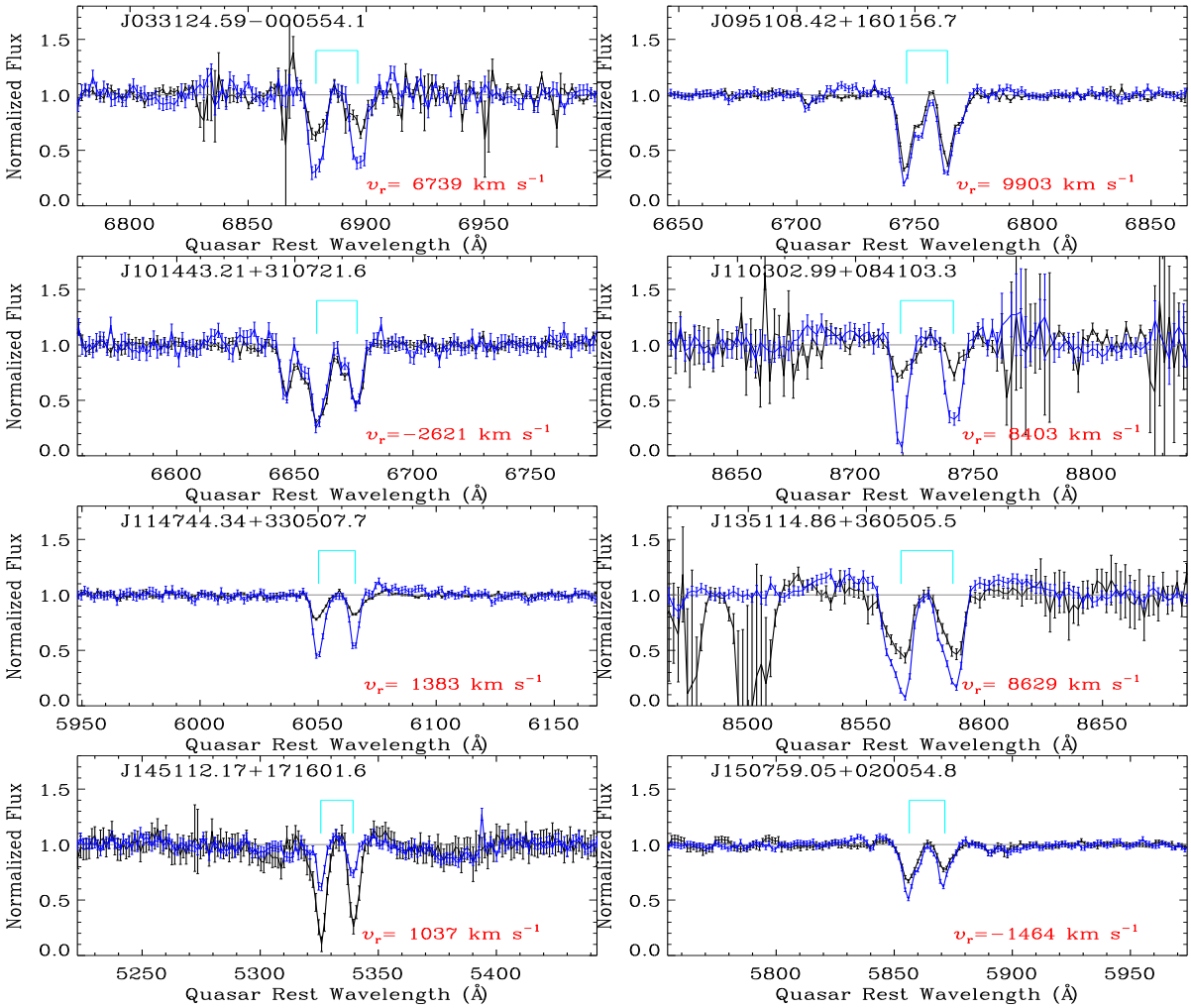

Fig. 10 The variable Mg II NALs in the normalized spectra. The black lines are for the LAMOST spectra, and the blue ones are for the SDSS spectra. The variable Mg II NALs are labeled with cyan lines. The v_r values are the velocity offsets of the variable Mg II NALs relative to the quasar emission line redshifts.

$3\sigma_w$ and $W_r^{\lambda 2803} \geq 2\sigma_w$). For the other $347 - 132 = 215$ Mg II NALs that were obviously observed in the SDSS spectra but not detected by methods applied in this paper, we have also measured their absorption strengths or upper limits on absorption strengths. We compute the changes in Mg II NALs between the LAMOST and SDSS observations with $\Delta W_r = W_{\rm r}^{\rm LAMOST} - W_{\rm r}^{\rm SDSS}$, where $W_{\rm r}^{\rm LAMOST}$ and $W_{\rm r}^{\rm SDSS}$ are for the absorption strengths measured from the spectra of LAMOST and SDSS, respectively. Figure 9 shows the changes in the Mg II NALs between the LAMOST and SDSS observations. We find that there are eight Mg II NALs with $|\Delta W_r^{\lambda 2796}| \geq 3\sigma_w$ (called variable Mg II NALs), which were changed on timescales of $\Delta{\rm MJD}/(1+{\rm z_{em}}) = 359$ — 2819 d. The time intervals and velocity offsets of the variable Mg II NALs are signified with red lines in Figures 8 and 6, respectively. The spectra of the variable Mg II NALs are displayed in Figure 10.

The associated Mg II NALs are located within the vicinities of quasar central regions. Under the model of photoionization equilibrium, the gas column densities of associated Mg II NALs can be changed by variations in quasar emissions (e.g., Narayanan et al. 2004; Chen et al. 2018b, 2019b, and references therein). On the other hand, the bulk movements of Mg II absorbing clouds relative to quasar sightlines can give rise to changes in the efficient coverage fractions of Mg II absorbing clouds to quasar center regions, and thus can also result in changes in the total column densities of Mg II NALs and produce variable Mg II NALs. The changes in quasar emissions cannot play a role in changing the gas column densities of intervening Mg II NALs, since they are far away from quasar systems. In addition, on a timescale of a few years, it is difficult for the bulk movements to obviously change the total column densities of intervening Mg II NALs, since the intervening Mg II NALs usually have low densities and very large sizes. Therefore, most of the variable Mg II NALs are often expected to be physically associated with quasar systems.

Assuming the bulk movements of Mg II absorbing clouds relative to quasar sightlines result in variable Mg II NALs and also that the variable Mg II absorbers are located around the Mg II broad emission line region (BELR), the maximum speed ($\upsilon_{\rm max}$) of the variable Mg II absorber across the quasar sightline can be on the order of the rotational speed, which obeys Kepler's third law. That is, $\upsilon_{\rm max} \sim \sqrt{GM_{\rm BH}/R_{\rm BELR}}$. We directly take the values of black hole mass ($M_{\rm BH}$) and continuum luminosities at 3000 Å (L_{3000}) from Yao et al. (2019). Using the radius-luminosity relation (Panda et al. 2019), we derive the $R_{\rm BELR}$ from L_{3000}, and thus estimate the maximum speeds of the variable Mg II absorbers across the quasar sightline with $\upsilon_{\rm max} = \sqrt{GM_{\rm BH}/R_{\rm BELR}}$. The derived $R_{\rm BELR}$ and $\upsilon_{\rm max}$ are provided in Table 2. For an optically thick and geometrically thin accretion disk, the UV continuum emission mainly comes from the inner accretion disk, which has a size scale of $D_{\rm cont} \sim 5R_{\rm S} = 10GM_{\rm BH}/c^2$ (Wise et al. 2004; Misawa et al. 2005). The derived $D_{\rm cont}$ values are provided in Table 2. If the variable Mg II absorbers travel with the speed $\upsilon_{\rm max}$ in time ($t_{\rm across}$) between two observations of SDSS and LAMOST, we can estimate the distances across the absorbers with $D_{\rm across} = \upsilon_{\rm max} \times t_{\rm across}$. The results are provided in Table 2. It is clearly seen that the distances across the absorbers are much larger than the sizes of UV continuum emission sources. If we assume that such distances of variable Mg II absorbers are similar to the sizes of the UV continuum emission sources during two observations of SDSS and LAMOST, we can estimate the transverse speeds of the absorbers via $\upsilon_{\rm tr} = D_{\rm cont}/t_{\rm across}$. The results are provided in Table 2. These derived transverse speeds seem to provide a reasonable explanation for the origin of variable Mg II NALs.

Changes in quasar emissions are one of the important mechanisms driving changes in associated QALs (e.g., Wang et al. 2015; He et al. 2017; Chen et al. 2018a; Lu et al. 2018; Lu & Lin 2018; Chen et al. 2019b). Decreasing emission can result in recombinations of Mg III $\rightarrow$ Mg II and Mg II $\rightarrow$ Mg I, and increasing emission can bring about photoionizations of Mg I $\rightarrow$ Mg II and Mg II $\rightarrow$ Mg III. It is a pity that we cannot investigate the changes in quasar emissions in this paper, since the LAMOST project only provides rough flux calibrations for their quasar spectra (Ai et al. 2016; Dong et al. 2018; Yao et al. 2019). We assume Mg II and Mg III are the dominant ionization states of Mg for the weakened and strengthened Mg II NALs, respectively. Taking the time between two observations of the SDSS and LAMOST as the upper limit of the recombination time of absorbing gas, we can estimate the electron density with $n_e \gtrsim (\alpha_r t_{\rm across})^{-1}$ (e.g., Narayanan et al. 2004), where α_r is the recombination coefficient. Adopting $\alpha_r = 8.8 \times 10^{-13}$ cm^3 s^{-1} for Mg II $\rightarrow$ Mg I and $\alpha_r = 3.5 \times 10^{-12}$ cm^3 s^{-1} for Mg III $\rightarrow$ Mg II (Shull & van Steenberg 1982), we can obtain the lower limit for the electron density of absorbing gas. The results are provided in Table 2.

4 SUMMARY

Relying on Data Releases 1–5 of quasar catalogs from LAMOST, this paper has collected 12 317 quasars with median S/N $>$ 3 pixel^{-1} to search for Mg II NALs in the LAMOST spectral data from blue wings $\upsilon_r = 10\,000$ km s^{-1} to red wings of Mg II emission lines. We detected

Table 2 The Parameters of Quasar Center Regions and Absorbers of the Variable Mg II

LAMOST name	$M_{\rm BH}$ $M_\odot$	L_{3000} $\rm erg\,s^{-1}$	$R_{\rm BELR}$ pc	$D_{\rm cont}$ 10^{15} cm	$D_{\rm across}$ 10^{15} cm	$\upsilon_{\rm max}$ $\rm km\,s^{-1}$	$\upsilon_{\rm tr}$ $\rm km\,s^{-1}$	$n_{\rm e}$ $\rm cm^{-3}$
033124.59–000554.1	8.486	45.813	0.291	0.451	39.965	2126	24	0.604
095108.42+160156.7	9.280	46.350	0.603	2.813	42.531	3685	244	0.985
101443.21+310721.6	9.027	45.276	0.140	1.568	77.015	5706	116	0.842
110302.99+084103.3	8.863	45.714	0.254	1.076	10.881	3510	347	3.666
114744.34+330507.7	8.522	45.763	0.272	0.49	32.119	2292	35	0.811
135114.86+360505.5	9.365	45.894	0.325	3.417	28.681	5536	660	2.193
145112.17+171601.6	—	45.351	0.155	—	—	—	—	0.188
150759.05+020054.8	—	—	—	—	—	—	—	0.467

217 Mg II NALs with $W_r^{\lambda2796} \geq 3\sigma_w$ and $W_r^{\lambda2803} \geq 2\sigma_w$, which are in a redshift range of $0.4554 \leq z_{\rm abs} \leq 2.1110$.

Among the 12 317 quasars utilized to search for Mg II NALs in this paper, 6427 quasars were previously observed by SDSS. For the quasars observed by both LAMOST and SDSS, 347 and 135 Mg II NALs $W_r^{\lambda2796} \geq 3\sigma_w$ and $W_r^{\lambda2803} \geq 2\sigma_w$ were visible in the SDSS and LAMOST spectra, respectively. Among the 135 Mg II NALs present in the LAMOST spectra, three Mg II NALs were missed in the SDSS spectra. Among the 347 Mg II NALs imprinted in the SDSS spectra, 215 Mg II NALs were missed in the LAMOST spectra. The missed Mg II NALs are mainly due to the low S/Ns of corresponding spectra. Among the Mg II NALs seen in the SDSS or LAMOST spectra, we find that eight Mg II NALs have been obviously changed with $|\Delta W_r^{\lambda2796}| \geq 3\sigma_w$ in the time intervals between the SDSS and LAMOST observations. These variable Mg II NALs are probably associated with quasar outflows.

Acknowledgements This work was supported by the Guangxi Natural Science Foundation (2018GXNSFAA050001, 2019GXNSFFA245008 and GKAD19245136), the Scientific Research Project of Guangxi University for Nationalities (2018KJQD01) and the National Natural Science Foundation of China (Grant Nos. 11763001, 11363001 and 12073007).

References

Abazajian, K. N., Adelman-McCarthy, J. K., Agüeros, M. A., et al. 2009, ApJS, 182, 543
Ai, Y. L., Wu, X.-B., Yang, J., et al. 2016, AJ, 151, 24
Alam, S., Albareti, F. D., Allende Prieto, C., et al. 2015, ApJS, 219, 12
Bahcall, J. N., Peterson, B. A., & Schmidt, M. 1966, ApJ, 145, 369
Bahcall, J. N., & Salpeter, E. E. 1965, ApJ, 142, 1677
Bahcall, J. N., & Salpeter, E. E. 1966, ApJ, 144, 847
Bergeron, J. 1986, A&A, 155, L8
Bergeron, J., & Boissé, P. 1991, A&A, 243, 344
Bowen, D. V., Hennawi, J. F., Ménard, B., et al. 2006, ApJ, 645, L105
Charlton, J. C., & Churchill, C. W. 1996, ApJ, 465, 631
Chen, H.-W. 2017, The Circumgalactic Medium in Massive Halos, eds. A. Fox & R. Davé, 430, Gas Accretion onto Galaxies (Springer International Publishing AG, 2017), 167
Chen, H.-W., Helsby, J. E., Gauthier, J.-R., et al. 2010, ApJ, 714, 1521
Chen, Z.-F., Gu, Q.-S., Chen, Y.-M., & Cao, Y. 2015a, MNRAS, 450, 3904
Chen, Z.-F., Gu, Q.-S., & Chen, Y.-M. 2015b, ApJS, 221, 32
Chen, Z.-F., & Pan, D.-S. 2017, ApJ, 848, 79
Chen, Z.-F., Huang, W.-R., Pang, T.-T., et al. 2018a, ApJS, 235, 11
Chen, Z.-F., Pang, T.-T., He, B., & Huang, Y. 2018b, ApJS, 236, 39
Chen, Z.-F., Yi, S.-X., Pang, T.-T., et al. 2019a, ApJS, 244, 36
Chen, Z.-F., Yi, S.-X., Pang, T.-T., et al. 2019b, ApJS, 243, 2
Cui, X.-Q., Zhao, Y.-H., Chu, Y.-Q., et al. 2012, RAA (Research in Astronomy and Astrophysics), 12, 1197
Dong, X. Y., Wu, X.-B., Ai, Y. L., et al. 2018, AJ, 155, 189
Farina, E. P., Falomo, R., Scarpa, R., et al. 2014, MNRAS, 441, 886
Hamann, F. 1997, ApJS, 109, 279
He, Z., Wang, T., Zhou, H., et al. 2017, ApJS, 229, 22
Kacprzak, G. G., Churchill, C. W., Ceverino, D., et al. 2010, ApJ, 711, 533
Lanzetta, K. M., & Bowen, D. 1990, ApJ, 357, 321
Le Brun, V., Bergeron, J., Boisse, P., & Christian, C. 1993, A&A, 279, 33
Lu, W.-J., & Lin, Y.-R. 2018, MNRAS, 474, 3397
Lu, W.-J., Lin, Y.-R., & Qin, Y.-P. 2018, MNRAS, 473, L106
Lundgren, B. F., Brunner, R. J., York, D. G., et al. 2009, ApJ, 698, 819
Luo, A. L., Zhang, H.-T., Zhao, Y.-H., et al. 2012, RAA (Research in Astronomy and Astrophysics), 12, 1243
Luo, A. L., Zhao, Y.-H., Zhao, G., et al. 2015, RAA (Research in Astronomy and Astrophysics), 15, 1095
Misawa, T., Charlton, J. C., & Eracleous, M. 2014, ApJ, 792, 77
Mo, H. J., & Miralda-Escude, J. 1996, ApJ, 469, 589
Narayanan, D., Hamann, F., Barlow, T., et al. 2004, ApJ, 601, 715
Nestor, D. B., Turnshek, D. A., & Rao, S. M. 2005, ApJ, 628, 637
Nestor, D., Hamann, F., & Rodriguez Hidalgo, P. 2008, MNRAS, 386, 2055

Nestor, D. B., Johnson, B. D., Wild, V., et al. 2011, MNRAS, 412, 1559
Panda, S., Martínez-Aldama, M. L., & Zajaček, M. 2019, Frontiers in Astronomy and Space Sciences, 6, 75
Qin, Y.-P., Chen, Z.-F., Lü, L.-Z., et al. 2013, PASJ, 65, 8
Quider, A. M., Nestor, D. B., Turnshek, D. A., et al. 2011, AJ, 141, 137
Rao, S. M., & Turnshek, D. A. 2000, ApJS, 130, 1
Seyffert, E. N., Cooksey, K. L., Simcoe, R. A., et al. 2013, ApJ, 779, 161
Shen, Y., & Ménard, B. 2012, ApJ, 748, 131
Shull, J. M., & van Steenberg, M. 1982, ApJS, 48, 95
Strömgren, B. 1948, ApJ, 108, 242
Tinker, J. L., & Chen, H.-W. 2008, ApJ, 679, 1218
Vanden Berk, D., Khare, P., York, D. G., et al. 2008, ApJ, 679, 239
Wang, T., Yang, C., Wang, H., & Ferland , G. 2015, ApJ, 814, 150
Weymann, R. J., Williams, R. E., Peterson, B. M., & Turnshek, D. A. 1979, ApJ, 234, 33
Wild, V., Kauffmann, G., White, S., et al. 2008, MNRAS, 388, 227
Wu, X.-B., Chen, Z.-Y., Jia, Z.-D., et al. 2010a, RAA (Research in Astronomy and Astrophysics), 10, 737
Wu, X.-B., Jia, Z.-D., Chen, Z.-Y., et al. 2010b, RAA (Research in Astronomy and Astrophysics), 10, 745
Yao, S., Wu, X.-B., Ai, Y. L., et al. 2019, ApJS, 240, 6
York, D. G., Adelman, J., Anderson, John E., J., et al. 2000, AJ, 120, 1579
Zhao, G., Zhao, Y.-H., Chu, Y.-Q., Jing, Y.-P., & Deng, L.-C. 2012, RAA (Research in Astronomy and Astrophysics), 12, 723
Zhu, G., & Ménard, B. 2013, ApJ, 770, 130